12 Apr 2023

Epitaxial Single-Domain Cu-BTC Metal-Organic Framework Thin Films and Foils by Electrochemical Conversion of Cuprous Oxide

Xiaoting Zhang

Bin Luo

Avishek Banik

John Z. Tubbesing

et. al. For a complete list of authors, see https://scholarsmine.mst.edu/chem_facwork/3378

Recommended Citation

X. Zhang et al., "Epitaxial Single-Domain Cu-BTC Metal-Organic Framework Thin Films and Foils by Electrochemical Conversion of Cuprous Oxide," *ACS Applied Materials and Interfaces*, vol. 15, no. 14, pp. 18440 - 18449, American Chemical Society, Apr 2023.
The definitive version is available at https://doi.org/10.1021/acsami.2c22983

ACS APPLIED MATERIALS & INTERFACES

www.acsami.org

Research Article

Epitaxial Single-Domain Cu-BTC Metal–Organic Framework Thin Films and Foils by Electrochemical Conversion of Cuprous Oxide

Xiaoting Zhang, Bin Luo, Avishek Banik, John Z. Tubbesing, and Jay A. Switzer*

Cite This: *ACS Appl. Mater. Interfaces* 2023, 15, 18440–18449

Read Online

ACCESS | Metrics & More | Article Recommendations | Supporting Information

ABSTRACT: Metal–organic frameworks (MOFs) are an important class of crystalline porous materials with extensive chemical and structural merits. However, the fabrication of MOF thin films oriented along all crystallographic axes to achieve well-aligned nanopores and nanochannels with uniform apertures remains a challenge. Here, we achieved highly crystalline single-domain MOF thin films with the [111] out-of-plane orientation by electrochemical conversion of cuprous oxide. Copper(II)-benzene-1,3,5-tricarboxylate, $Cu_3(BTC)_2$ (referred to as Cu-BTC), is a well-known metal–organic open framework material with a cubic crystal system. Epitaxial Cu-BTC(111) thin films were manufactured by electrochemical oxidation of Cu_2O(111) films electrodeposited on single-crystal Au(111). The Cu-BTC(111) shows an in-plane antiparallel relationship with the precursor Cu_2O(111) with a −0.91% coincidence site lattice mismatch. A plausible mechanism was proposed for the electrochemical conversion of Cu_2O into Cu-BTC, indicating formation of intermediate CuO, growth of Cu-BTC islands, and termination with coalesce into a dense film with a limiting thickness of about 740 nm. The Faradaic efficiency for the electrochemical conversion was 63%. In addition, epitaxial Cu-BTC(111) foils were fabricated by epitaxial lift-off following the electrochemical etching of residual Cu_2O underneath the Cu-BTC. It was also demonstrated that Cu-BTC(111) films with two in-plane domains and textured Cu-BTC(111) films can be achieved on a large scale using electrodeposited Au/Si and Au-coated glass as low-cost substrates.

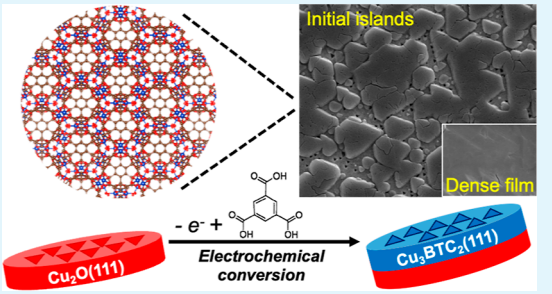

KEYWORDS: *metal–organic frameworks, single-domain, Cu-BTC, electrochemical conversion, epitaxial lift-off, foils, cuprous oxide*

INTRODUCTION

Epitaxy is the growth of crystals on a single-crystal substrate that determines their orientation.[1,2] It can be used to produce films with a level of perfection that approaches that of single crystals. Epitaxy is particularly important for manufacturing single-crystal-like metal and semiconductor films to reduce the defect sites at interfaces and grain boundaries and thus optimize their opto-electronic properties and device performance. Metal–organic frameworks (MOFs) built from metal ions coordinated by organic ligands to form rigid topological networks[3−5] are compelling highly porous crystalline materials for gas storage and separation,[6,7] catalysis,[8,9] sensors,[10−12] and energy storage and conversion.[13] Epitaxial MOF thin films with highly oriented nanopore openings and channels are desired for selective adsorption/separation[14−16] and enantioselectivity,[17,18] as well as encapsulation of various guests such as metallic catalysts,[19] quantum dots,[20,21] and dye molecules.[22,23] $[Cu_3(BTC)_2(H_2O)_3]_n$ (Cu-BTC, HKUST-1)[24] is one of the most well-studied MOF materials. It is constructed from dimeric Cu(II) units bridged by benzene-1,3,5-tricarboxylate (BTC) ligands with a face-centered cubic lattice (space group, $Fm\bar{3}m$). While many synthetic routes exist for the production of bulk Cu-BTC powders, to our knowledge, there are no examples of epitaxial Cu-BTC thin films which have both a single out-of-plane and in-plane orientation. This limitation has blocked the full exploitation of this material in sensing, catalytic, and electrical applications.[25−27]

Electrochemical epitaxy including electrodeposition and electro-conversion is a low-cost and scalable technique for growing highly ordered thin films.[28−32] The conventional electrochemical method using Cu metal as the precursor can only produce polycrystalline Cu-BTC films by anodic dissolution–reprecipitation.[33] Textured Cu-BTC films with only out-of-plane order can be produced by layer-by-layer liquid phase epitaxy using a surface-functionalized Si or Au substrate by functional groups (such as −COOH or −OH). Although the appropriate nucleation sites were provided, they failed to show in-plane order.[34,35] The Takahashi group fabricated Cu-BTC thin films by chemical conversion of aligned $Cu(OH)_2$(100) nanobelts. The Cu-BTC showed preferential out-of-plane lattice planes of {111} with the

Received: December 22, 2022
Accepted: March 23, 2023
Published: April 3, 2023

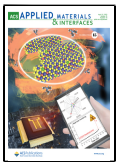

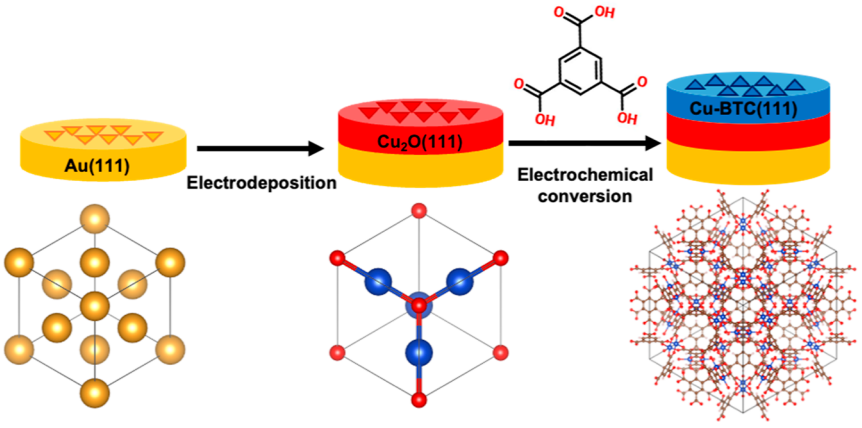

Figure 1. Schematic for electrochemical manufacturing of epitaxial single-domain Cu-BTC thin films.

coexistence of {110}, and both exhibited in-plane epitaxial relationships with $Cu(OH)_2(100)$.[23,36] However, it would be challenging to produce wafer-scale Cu-BTC from manually aligned $Cu(OH)_2$ nanobelts, and Cu-BTC thin films with a single out-of-plane orientation and in-plane order have not been achieved. Here, we develop a novel strategy to fabricate epitaxial Cu-BTC(111) thin films from $Cu_2O(111)$ films on Au(111) by electrochemical conversion. Despite a considerable lattice mismatch between Cu_2O and Cu-BTC, there is an epitaxial correlation between the orientation of $Cu_2O(111)$ and Cu-BTC(111) after conversion. The epitaxial Cu-BTC thin films show out-of-plane order with only {111} lattice planes, providing well-aligned 3.5 Å triangular windows along the [111] direction.[37] Remarkably, this Cu-BTC(111) film exhibits in-plane order with a single in-plane domain that is in an antiparallel relation to the Cu_2O. We also demonstrate a pathway to produce epitaxial Cu-BTC foils from the Cu-BTC/Cu_2O system by electrochemical etching. The electrochemically manufactured epitaxial single-domain Cu-BTC thin films exhibit a highly ordered arrangement of nanopores/nanochannels in all three crystallographic dimensions ($x-y$ plane and z-axis) and should provide a new platform for fundamental and technical studies of ordered MOF film materials.

EXPERIMENTAL SECTION

Electrodeposition of the Cu_2O Film. Cu_2O was electrodeposited from a stirred aqueous solution containing 0.2 M $CuSO_4$, 0.2 M L (+)-tartaric acid, and 3 M NaOH.[38] The working electrode was a 1 cm diameter Au(111) single crystal purchased from Princeton Scientific Co. The electrodeposition was conducted at a constant cathodic current density of 1 mA/cm^2 at 30 °C using an Ag/AgCl reference electrode and an Au coil as the counter electrode.

Electrochemical Conversion of Cu_2O into Cu-BTC. Cu_2O was electrochemically converted into Cu-BTC in an unstirred solution of EtOH/H_2O (70:30 vol %) containing 50 mM H_3BTC (benzene-1,3,5-tricarboxylic acid) and 100 mM $LiClO_4$. The electrochemical conversion was performed at 50 °C with a constant potential of +0.5 V versus Ag/AgCl.

Fabrication of Cu-BTC Foil. A Cu-BTC foil was produced by electrochemically oxidizing the as-prepared Cu-BTC/Cu_2O/Au to etch the Cu_2O layer in an aqueous solution (pH 4 adjusted by H_2SO_4) containing 100 mM Na_2SO_4 with a constant potential of +0.2 V versus Ag/AgCl applied for 40−100 s at room temperature. The Cu-BTC foil was then peeled from the Au substrate with a commercial (3M) adhesive tape.

Cyclic Voltammetry Measurements. Cyclic voltammograms were conducted on Cu and Cu_2O deposited onto 1 cm × 1 cm Au-coated glass in unstirred solutions at 50 °C with the scan rate of 10 mV/s. Au-coated glass was out-of-plane ordered Au(111) (without in-plane order) coated on a titanium adhesion layer on the glass and was purchased from DRLi Deposition Research Lab, Inc.

XRD Measurements and Interface Models. All X-ray diffraction (XRD) measurements were performed on a high-resolution Philips X-Pert MRD diffractometer with Cu Kα1 radiation source (λ = 1.54056 Å). XRD patterns (2θ scans) were acquired using a 2-bounce Ge(220) hybrid monochromator with a Ni 0.125 mm automatic beam attenuator as the primary optic module and a 0.18° parallel plate collimator as the secondary optic module. Rocking curves were performed using the same 2-bounce Ge(220) hybrid monochromator with rocking curve diffracted beam optics. Pole figures and azimuthal scans were done in point focus mode using a crossed-slit collimator with a 2 mm divergence slit and a 2 mm mask and a 0.27° parallel plate collimator. A β-Ni filter was used for the Cu-BTC pole figure and azimuthal scans, and a 0.1 mm Cu attenuator was used for all others. Interface models were constructed by VESTA 3.4.0 software.

SEM Measurements. Plan-view and cross-sectional scanning electron microscopy (SEM) images were acquired by a FEI Helios Nanolab DualBeam scanning electron microscope with an accelerating voltage of 5 kV and beam current of 43 pA for all samples.

EQCM Measurements. Electrochemical quartz crystal microbalance (EQCM) (Stanford Research Systems QCM200) was utilized to simultaneously monitor the frequency change and current density during deposition and conversion experiments. Au-sputtered quartz crystals served as the working electrode for the EQCM measurements.

XPS and FTIR Measurements. Samples were prepared for X-ray photoelectron spectroscopy (XPS) and Fourier-transform infrared spectroscopy (FTIR) measurements. Cu_2O/Au/glass was made by electrodepositing Cu_2O on Au-coated glass. Oxidized-Cu_2O/Au/glass was prepared by oxidizing Cu_2O/Au/glass in the solution of EtOH/H_2O (70:30 vol %) containing 100 mM $LiClO_4$ with a constant potential of +0.5 V versus Ag/AgCl at 50 °C. CuO/Au/glass was obtained by depositing CuO on Au-coated glass using our previously reported method.[39] $Cu(OH)_2$/Au/glass was prepared by oxidizing Cu on Au-coated glass following the reported methods.[40] XPS investigations were run on a Thermo Scientific Nexsa X-ray photoelectron spectrometer using monochromatic Al Kα radiation (1486.6 eV). The XPS spectra were resolved by using Gaussian peaks after a Shirley background subtraction. FTIR measurements were done in a Nicolet iS50 FTIR using the ATR attachment.

RESULTS AND DISCUSSION

The scheme used to produce epitaxial single-domain Cu-BTC films is shown in Figure 1. The epitaxial Cu_2O films were electrodeposited onto single-crystal Au, and these Cu_2O films with out-of-plane and in-plane order served as the precursor to produce Cu-BTC films by electrochemical oxidation in electrolytes containing H_3BTC. Although Cu-BTC has a

https://doi.org/10.1021/acsami.2c22983
ACS Appl. Mater. Interfaces 2023, 15, 18440−18449

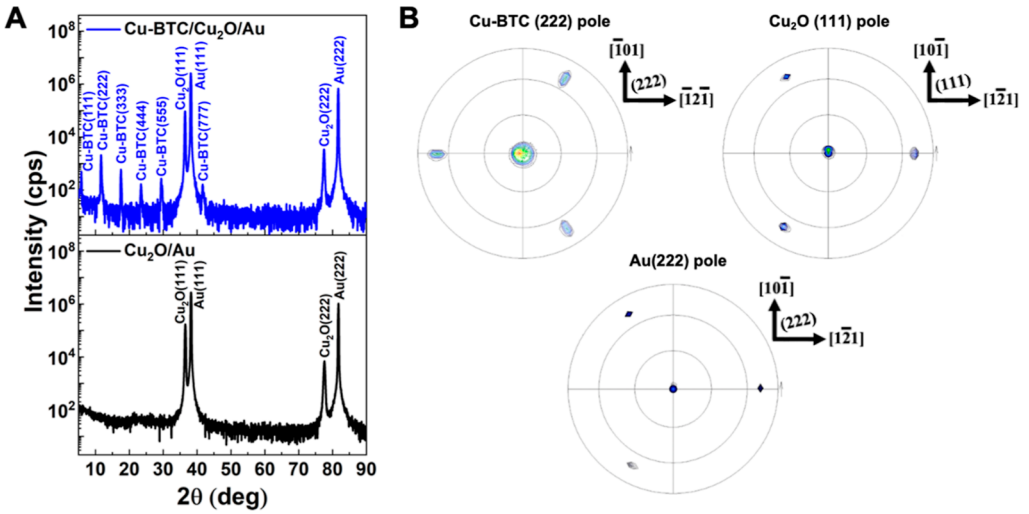

Figure 2. XRD analysis of the epitaxial Cu-BTC/Cu_2O/Au film. (A) XRD patterns of Cu-BTC/Cu_2O/Au(111) and Cu_2O/Au(111). (B) (222) pole figure of Cu-BTC, (111) pole figure of Cu_2O, and (222) pole figure of Au.

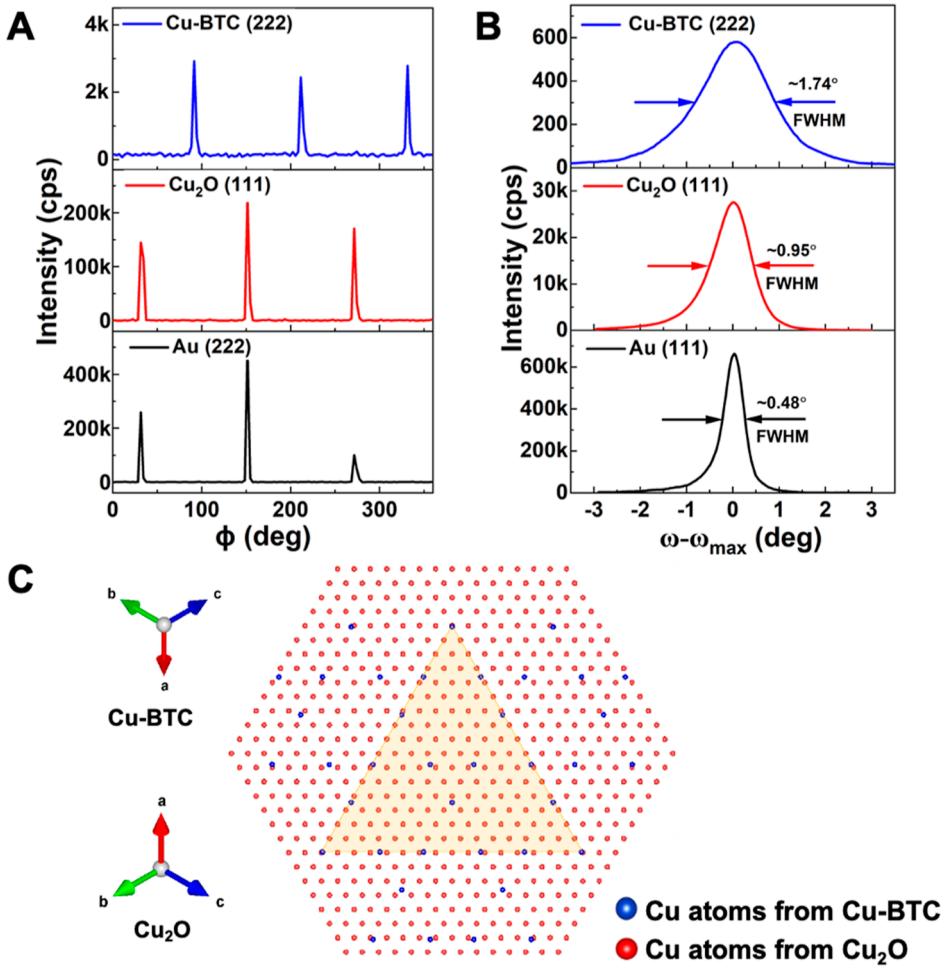

Figure 3. Epitaxial relationship and interface models of Cu-BTC(111) on Cu_2O/Au(111) substrate. (A) Azimuthal scans of Cu-BTC(222), Cu_2O(111), and Au(222) at tilt angle χ = 70.53°. (B) X-ray rocking curves of the (222) plane of Cu-BTC and (111) plane of Cu_2O and Au. (C) In-plane interface model of Cu (blue) atoms of Cu-BTC(111) with Cu (red) atoms of Cu_2O(111) with the Cu-BTC lattice rotated 180° in-plane with respect to the Cu_2O lattice. 17 Cu atoms of Cu_2O coincide with 6 Cu atoms of Cu-BTC with a CSL mismatch of −0.91%.

large unit cell compared to that of Cu_2O, and the volume per Cu atom in Cu-BTC is 20-fold of that in Cu_2O (Figure S1 and Table S1), the epitaxial electrochemical conversion occurred from Cu_2O to Cu-BTC.

The out-of-plane orientation of the Cu_2O films and Cu-BTC films electrochemically converted from the Cu_2O was determined by X-ray 2θ scans. Figure 2A shows the XRD patterns of the precursor Cu_2O film deposited on single-crystal

https://doi.org/10.1021/acsami.2c22983
ACS Appl. Mater. Interfaces 2023, 15, 18440−18449

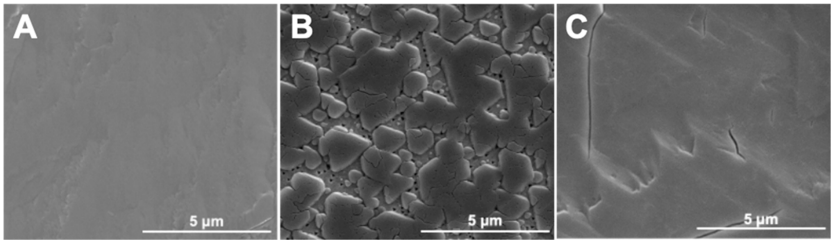

Figure 4. Plan-view SEM images of (A) as-deposited $Cu_2O(111)$ film on Au(111), (B) Cu-BTC(111) film after conversion of $Cu_2O(111)$/Au(111) for 10 s, and (C) Cu-BTC(111) film after conversion of $Cu_2O(111)$/Au(111) for 50 s.

Au(111) and the resulting Cu-BTC film after electrochemical conversion. The Cu_2O films grow with a [111] out-of-plane orientation on the Au(111) surface. The Cu-BTC films follow the out-of-plane orientation of Cu_2O and only show peaks of the {111} family with no other crystallographic orientations, unlike earlier reports.[36] The precursor Cu_2O can be completely converted into Cu-BTC if the Cu_2O is thin enough (about 60 nm thick) as shown in Figures S2 and S3. However, when producing Cu-BTC films that are to be lifted off to produce Cu-BTC foils, a greater thickness (greater than 60 nm) is required for post-fabrication etching.

The in-plane orientation and the epitaxial relationship of Cu-BTC/Cu_2O/Au were determined by X-ray pole figures. All pole figures require a fixed 2θ angle while rotating the sample along azimuthal angles (ϕ) from 0 to 360° at a succession of tilt angles (χ) from 0 to 90°. For a given sample, the in-plane orientations are determined by selecting the appropriate 2θ angle for each material that is probed. The 2θ angle was set equal to the (222) reflection for Au, the (111) reflection for Cu_2O, and the (222) reflection for Cu-BTC. Figure 2B shows the (222) pole figure of Au, (111) pole figure of Cu_2O and (222) pole figure of Cu-BTC. Each pole figure had a center intense spot at χ = 0° and three sharp spots separated azimuthally by 120° at χ = 70.53°, consistent with a single domain of threefold symmetry in a cubic system. The intense center spot is attributed to the probed crystal plane (111) aligned with the surface (111) plane of the films when the tilt angle is 0°. The tilt angle of 70.53° corresponds to the angle between the surface (111) plane and the probed crystal planes $(11\bar{1})$, $(1\bar{1}1)$, and $(\bar{1}11)$. Note that it is also significant that epitaxial single-domain Cu_2O thin films were realized in our work because the material plays an important role in water splitting and photovoltaics.[41,42] The pole figure of Cu_2O maintained the same in-plane rotation with respect to the Au substrate indicating a parallel relationship. The Cu_2O and Cu-BTC pole figures showed that Cu-BTC was rotated 180° in-plane in relation to the precursor Cu_2O, demonstrating that antiparallel lattice planes were produced after conversion. The epitaxial relationship for single domain Cu-BTC on Cu_2O/Au is given by Cu-BTC$(111)[\bar{1}01]//Cu_2O(111)[10\bar{1}]//$Au-$(111)[10\bar{1}]$.

The epitaxial perfection and crystal quality of Cu-BTC(111) films of Cu_2O/Au were further investigated by azimuthal scans and X-ray rocking curves. Figure 3A shows azimuthal scans which were acquired by setting 2θ equal to the (222) reflection for Au, the (111) reflection for Cu_2O and the (222) reflection for Cu-BTC at χ = 70.53°. In each azimuthal scan, three peaks were observed consistent with the pole figures, illustrating the single domain in-plane ordering. The coincident peak positions correspond to the parallel relationship between Au and Cu_2O, and the peak shifts for Cu-BTC with respect to Cu_2O correspond to the antiparallel relationship between Cu_2O and Cu-BTC. Rocking curves were acquired to measure the mosaic spread because the full width at half maximum (FWHM) of the rocking curve is a measure of the standard deviation in the mosaic spread. Figure 3B shows the rocking curves recorded by rocking the sample at the diffraction angle of Au(111), $Cu_2O(111)$, and Cu-BTC(222). The FWHM is about 0.48° for Au(111), 0.95° for $Cu_2O(111)$, and 1.74° for Cu-BTC.

Considering the evident lattice difference between Cu-BTC(111) and the substrate $Cu_2O(111)$, it is necessary to address the lattice mismatch for a better understanding of their epitaxial relationship. The lattice mismatch can be defined as $[(a_{film} - a_{substrate})/a_{substrate}]$, where a is the lattice parameter. The Cu-BTC/Cu_2O system has a very large lattice mismatch of ~520%, which appears inconsistent with epitaxial growth. Figure 3C shows the plan view of the Cu-BTC(111) plane rotated 180° in relation to the $Cu_2O(111)$ plane with an interface model constructed by Cu atoms (blue) in the Cu-BTC(111) plane and Cu atoms (red) in the $Cu_2O(111)$ plane. Six Cu atoms of Cu-BTC align with 17 Cu atoms of Cu_2O, producing a coincidence site lattice (CSL) with a mismatch of −0.91%. This low CSL mismatch is consistent with the formation of epitaxial Cu-BTC(111) on $Cu_2O(111)$.

The crystal growth process of Cu-BTC films on Cu_2O was investigated by plan-view SEM. Figure 4 shows the surface morphology of electrodeposited Cu_2O films before conversion and Cu-BTC thin films after electrochemical conversion with differing conversion times. Cu_2O films as deposited on single-crystal Au(111) showed a featureless and smooth surface (Figure 4A). After a conversion for 10 s, Cu-BTC grew as islands with well-aligned triangular crystals, consistent with the three-fold symmetry of a single in-plane domain (Figure 4B). Also observed in the SEM micrograph are small triangular etch pits in the Cu_2O precursor film between the Cu-BTC islands. When the conversion reached to 50 s, Cu-BTC formed a featureless dense film and fully covered the surface of Cu_2O (Figure 4C). The dense, single-domain film is essentially a single crystal. For thinner Cu_2O films, the Cu-BTC grows as islands, with no Cu_2O remaining. This is shown in the SEM micrograph and X-ray results in Figure S3 for the complete conversion of a 40 nm thick film of Cu_2O, in which triangular islands of Cu-BTC are formed on Au(111). The thickness of Cu-BTC films was probed by cross-sectional SEM (Figure S4). The Cu-BTC islands formed by complete conversion of 40 nm thick Cu_2O reach a thickness of 710 ± 20 nm (Figure S4A). The Cu-BTC film converted from 250 nm thick Cu_2O with remanent Cu_2O underneath has a thickness of 690 ± 30 nm (Figure S4B).

To gain insights into the mechanism of electrochemical conversion of Cu_2O into Cu-BTC, the known method of electrochemical oxidization of Cu metal to produce Cu-BTC

https://doi.org/10.1021/acsami.2c22983
ACS Appl. Mater. Interfaces 2023, 15, 18440−18449

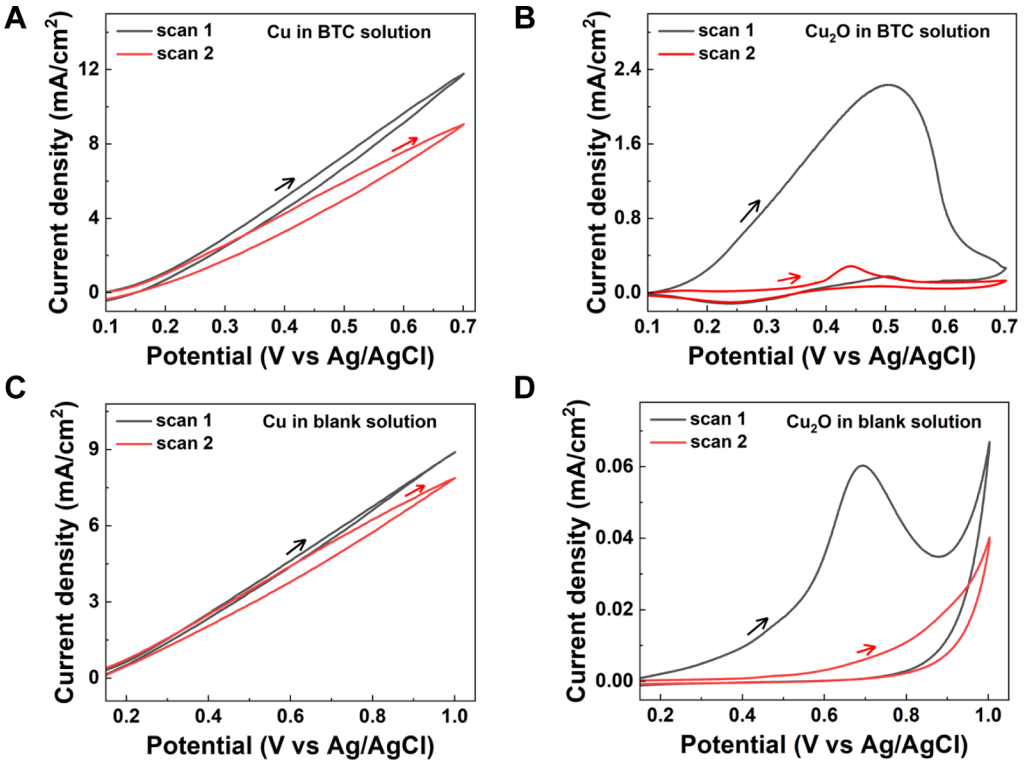

Figure 5. Cyclic voltammetry scans of (A) Cu/Au/glass and (B) Cu_2O/Au/glass electrode in the solution of EtOH/H_2O (70:30 vol %) containing 50 mM H_3BTC and 100 mM $LiClO_4$, and (C) Cu/Au/glass and (D) Cu_2O/Au/glass electrode in the solution of EtOH/H_2O (70:30 vol %) containing 100 mM $LiClO_4$. Scan rates of all CVs were 10 mV/s.

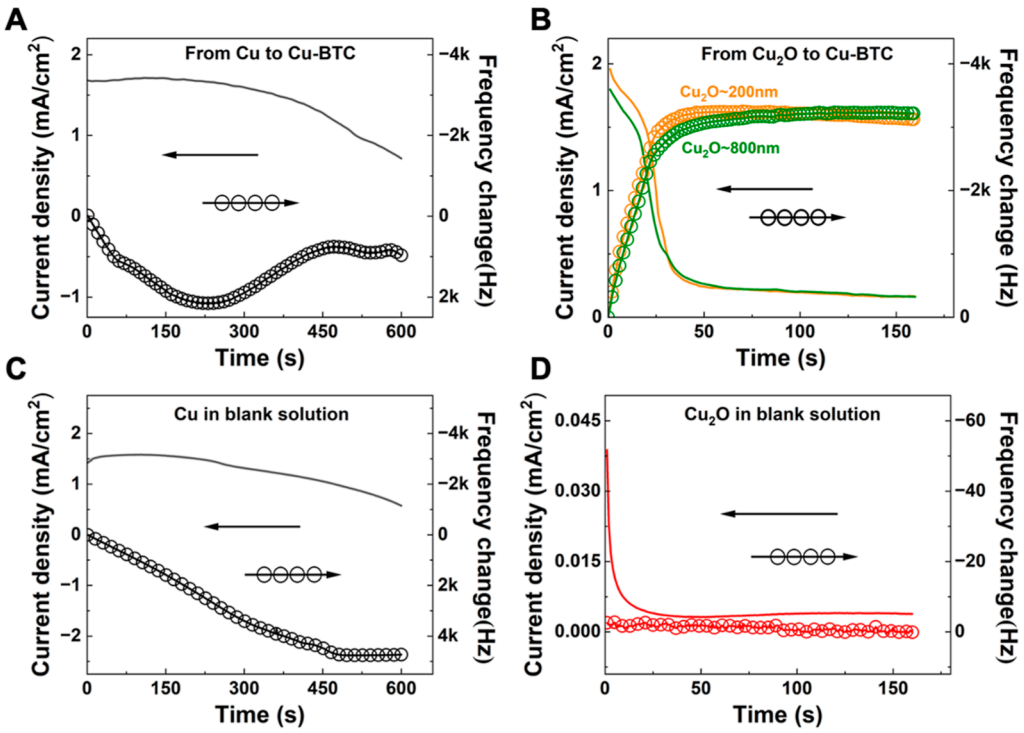

Figure 6. Current density (line, left axis) and frequency change (circles, right axis) as a function of elapsed time: (A) Cu and (B) Cu_2O in the bath of EtOH/H_2O (70:30 vol %) containing 100 mM $LiClO_4$ and 50 mM H_3BTC with a constant potential of +0.5 V vs Ag/AgCl at room temperature; (C) Cu and (D) Cu_2O in the bath of EtOH/H_2O (70:30 vol %) containing 100 mM $LiClO_4$ but no H_3BTC with a constant potential of +0.5 V vs Ag/AgCl at 50 °C.

was also investigated to represent the dissolution−redeposition mechanism.[33] It is worth noting that only polycrystalline Cu-BTC films can be produced by this method even when single-crystal Cu was used as the precursor and substrate (Figure S5).

https://doi.org/10.1021/acsami.2c22983
ACS Appl. Mater. Interfaces 2023, 15, 18440−18449

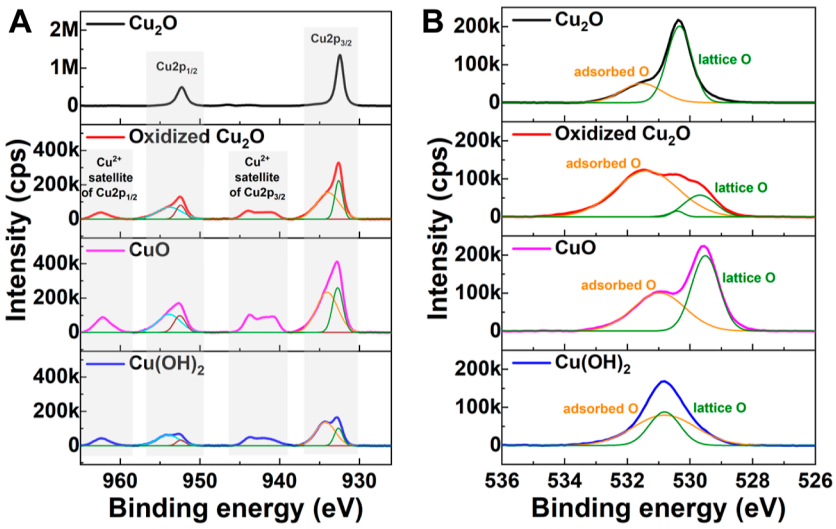

Figure 7. High-resolution XPS spectra of Cu_2O (black line), oxidized Cu_2O (red line), CuO (pink line), and $Cu(OH)_2$ (blue line). (A) Cu 2p and (B) O 1s binding energy ranges.

Cyclic voltammograms (CVs) were conducted to study the electrochemistry of both processes. Figure 5A shows the CVs conducted on the Cu film in electrolytes containing 50 mM H_3BTC and 100 mM $LiClO_4$. Both the first and second anodic scans indicated a dissolution process. Figure 5B shows the CVs conducted on a Cu_2O film in a solution containing 50 mM H_3BTC and 100 mM $LiClO_4$. An oxidation peak was observed in the first anodic scan at +0.50 V versus Ag/AgCl corresponding to the formation of Cu-BTC. The significant decay of the oxidation peak in the second anodic scan is due to blocking by the Cu-BTC produced in the first scan. The CV in blank solution on Cu also showed dissolving behavior in the first and second scan with high current density (Figure 5C). However, on Cu_2O there is a low current density oxidation peak observed at +0.70 V in the first scan but no peak in the second scan (Figure 5D), which suggests an oxidized layer formed on the surface which hindered any further oxidation of Cu_2O. The Cu_2O consumed to form the oxidized layer was calculated using Faraday's law to be 2 nm thick. This oxidized layer suggests a possible intermediate in the conversion of Cu_2O into Cu-BTC.

The mechanism was further investigated using the EQCM. In the EQCM experiment, an increase in frequency indicates a mass loss, and a decrease in frequency indicates a mass gain. Figure 6A shows the electrochemical oxidation of Cu metal to Cu-BTC. The frequency increased from the beginning due to the dissolution of Cu metal and then started to slowly decrease corresponding to the precipitation of Cu-BTC. Figure 6B shows the electrochemical oxidation of Cu_2O to Cu-BTC. The frequency and current density decreased sharply from the start, corresponding to the growth of Cu-BTC on the surface (as can be seen in Figure 4B). The frequency then came to a plateau with a residual current density of about 0.25 mA/cm^2 after about 50 s, corresponding to the termination of the conversion because the surface was fully covered by Cu-BTC (as can be seen in Figure 4C). The conversion of the Cu_2O with different thicknesses (200 and 800 nm) terminated at the same frequency change. The amount of Cu_2O consumed can be calculated from Faraday's law using the charge that is passed, and this can be compared with the thickness of Cu-BTC that is produced based on the Sauerbrey equation. For the 200 nm thick Cu_2O film, the anodic charge passed was 0.05 C/cm^2, corresponding to a depletion of 37 μg/cm^2 and a thickness loss of 63 nm. The mass change of Cu-BTC was 94 μg/cm^2, corresponding to a thickness of 770 nm, and a current efficiency of 62%. For the 800 nm thick Cu_2O film, the anodic charge passed was 0.046 C/cm^2, corresponding to a depletion of 33 μg/cm^2 and a thickness loss of 56 nm. The mass change of Cu-BTC was 87 μg/cm^2, corresponding to a thickness of 713 nm, and a current efficiency of 64.5%. Hence, the average decrease of thickness of Cu_2O was 60 nm, the average thickness of Cu-BTC produced was 742 nm, and the average current efficiency was 63%. The thickness of Cu-BTC that is calculated from the frequency change in the EQCM experiment agrees well with the thickness that was measured by cross-sectional SEM in Figure S4. In the conversion of Cu_2O into Cu-BTC, the mass increased from the beginning without a typical dissolution phase, which indicates the Cu-BTC was probably formed on the interface of the substrate/solution as the H_3BTC molecule reached the surface and reacted with the oxidized layer of Cu_2O. The EQCM in the blank solution (Figure 6C,D) further demonstrated that Cu significantly dissolved in the blank solution, whereas Cu_2O was passivated by the oxidized layer.

The oxidized layer as a possible intermediate was investigated by high-resolution XPS by comparing the surface of as-deposited Cu_2O, Cu_2O oxidized in the blank solution (oxidized Cu_2O), CuO, and $Cu(OH)_2$ films (Figure 7). In the Cu 2p spectrum (Figure 7A), oxidized Cu_2O shows broadened Cu $2p_{1/2}$ and Cu $2p_{3/2}$ peaks with shake-up satellites of Cu(II), which confirmed the formation of Cu(II) on the surface.[43] In the O 1s spectra (Figure 7B), there are two kinds of deconvolved peaks for each sample: one belongs to oxygen in the lattice (Cu−O) and the other one is due to adsorbed oxygen from surface hydroxyl and carbonyl species. The peaks of lattice oxygen of Cu_2O, CuO, and $Cu(OH)_2$ are 530.3, 529.5, and 530.9 eV, respectively. The deconvolved peaks of lattice oxygen of oxidized Cu_2O are a major peak at 529.7 eV and a minor peak at 530.3 eV. The major peak at 529.7 eV is attributed to CuO that forms upon oxidation of Cu_2O. The minor peak at 530.3 eV is attributed to the underlying Cu_2O substrate. The calculated thickness based on Faraday's law of

https://doi.org/10.1021/acsami.2c22983
ACS Appl. Mater. Interfaces 2023, 15, 18440−18449

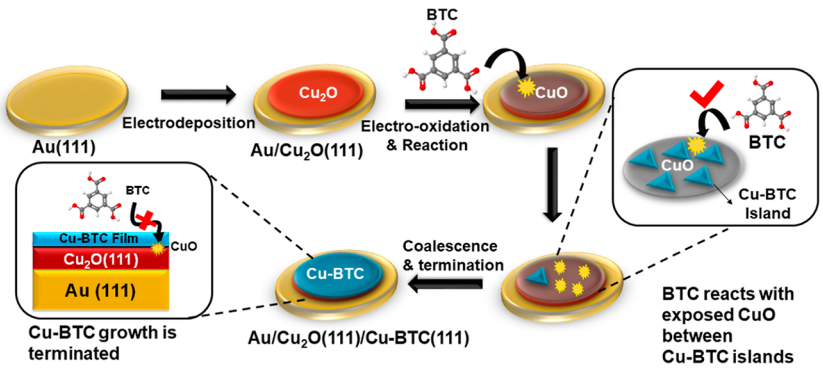

Figure 8. Plausible mechanism for electrochemical conversion from Cu_2O to Cu-BTC.

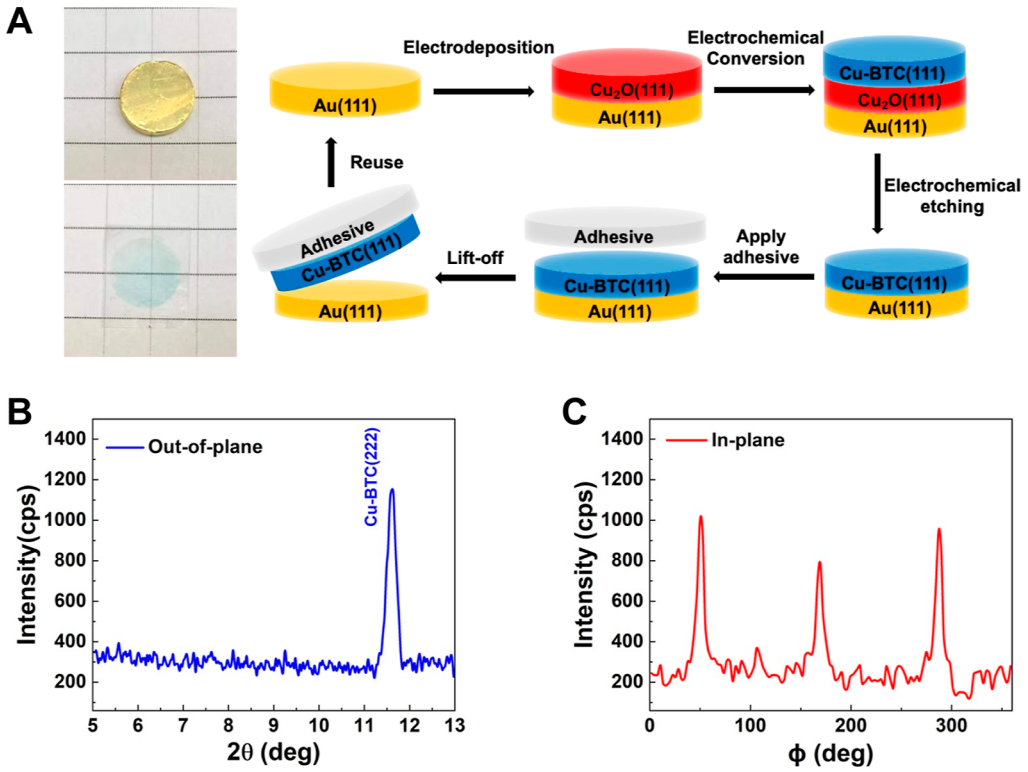

Figure 9. (A) Epitaxial lift-off of single-domain Cu-BTC foils: Cu_2O was electrochemically etched and Cu-BTC foils were detached by commercial tape. Optical photographs of the Au single crystal (top) and the Cu-BTC foil (bottom) are shown in the figure. (B) XRD pattern of the Cu-BTC foil. (C) Azimuthal scan of the Cu-BTC(222) foil at a tilt angle χ = 70.53°. The XRD results show that the single domain Cu-BTC foils are essentially single crystals.

the CuO layer is only 2.2 nm due to the 2.0 nm of Cu_2O that was consumed in the electrochemical oxidation, so the underlying Cu_2O will contribute to the signal. The oxidized layer was also verified by FTIR (Figure S6), and it was demonstrated that the CuO powder can react with H_3BTC to produce Cu-BTC (Figure S7).

Here, we propose a plausible mechanism for the electrochemical conversion of Cu_2O into Cu-BTC, as shown in the scheme in Figure 8. Cu_2O is electro-oxidized to form several molecular layers of CuO on the surface followed by the reaction of H_3BTC molecules with the surface CuO to form Cu-BTC that follows the orientation of the Cu_2O. The Cu-BTC crystals first form islands, and these islands grow as H_3BTC molecules continue to react with exposed CuO on the surface of Cu_2O. The conversion terminates once the surface is fully covered by Cu-BTC. We assume that the conversion terminates after the islands coalesce into a dense film, and the H_3BTC molecule is unable to diffuse along the 3.5 Å diameter channels of the [111]-oriented film. The mechanism may be more complex than the simple scheme shown in Figure 8. For example, small triangular etch pits that are observed in Cu_2O in Figure 4B suggest that the reaction of H_3BTC with CuO may not be uniform across the Cu_2O surface. There may be preferential etching, for instance, at defect sites.

At this point, we can compare our work on the electrochemical formation of Cu-BTC from Cu_2O to earlier work in which the MOF was produced from elemental Cu. Campagnol et al. showed that the Cu-BTC growth occurred at the Cu-BTC/solution interface.[33] They attributed the growth to the diffusion of $Cu_{(aq)}^{2+}$ ions along the pores of Cu-BTC to react with the H_3BTC molecule. In our case, we showed by EQCM (Figure 6D) that Cu_2O will not oxidize in the absence of

https://doi.org/10.1021/acsami.2c22983
ACS Appl. Mater. Interfaces 2023, 15, 18440−18449

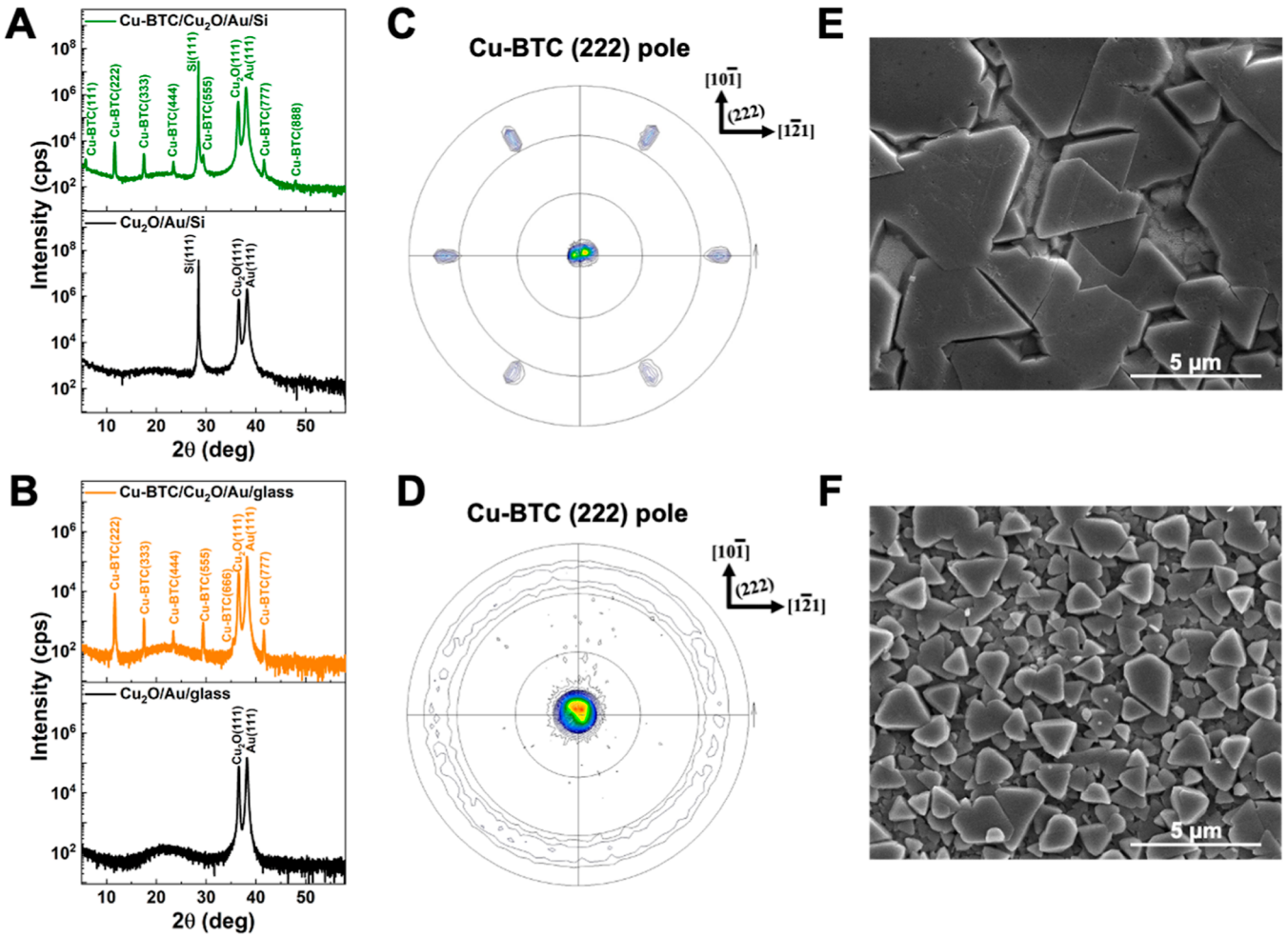

Figure 10. XRD patterns of (A) Cu-BTC/Cu_2O/Au/Si and Cu_2O/Au/Si, and (B) Cu-BTC/Cu_2O/Au/glass and Cu_2O/Au/glass. (222) pole of Cu-BTC of (C) Cu-BTC/Cu_2O/Au/Si, and (D) Cu-BTC/Cu_2O/Au/glass. Plan-view SEM images of (E) Cu-BTC/Cu_2O/Au/Si and (F) Cu-BTC/Cu_2O/Au/glass.

H_3BTC molecules to produce Cu^{2+} ions. The production of Cu-BTC only occurs at the exposed Cu_2O surface. Hence, once the material coalesces into a dense film, the reaction terminates (as shown in the EQCM results in Figure 6B).

Following the fabrication of Cu-BTC thin films, single-domain Cu-BTC(111) foils were also fabricated in our work from the Cu-BTC/Cu_2O system, as shown in Figure 9A. After highly ordered Cu-BTC(111) thin films were synthesized on Cu_2O/Au, the Cu_2O layer was removed by electrochemical etching. The Cu-BTC foils were then peeled off from the Au substrate by commercial tape. The out-of-plane orientation of the Cu-BTC foils was determined by XRD, with only the (222) peak observed (Figure 9B). The in-plane orientation was probed by azimuthal scans of the Cu-BTC(222) foil at a tilt angle $\chi = 70.53°$ with three peaks observed, demonstrating that the foil is still ordered with a single domain (Figure 9C).

To present more possibilities of ordered Cu-BTC thin films, epitaxial Cu-BTC with two in-plane domains and textured Cu-BTC with no in-plane order were also produced using low-cost and wafer-scalable commercial substrates Si and Au-coated glass. Cu-BTC films on Cu_2O/Au/Si and Cu-BTC films on Cu_2O/Au/glass both showed an out-of-plane [111] orientation (Figure 10A,B). Figure 10C shows the (222) pole figure of Cu-BTC on Cu_2O/Au/Si with six spots separated azimuthally by 60° at $\chi = 70.53°$, consistent with the two domains of threefold symmetry of the (111) plane; the second domain comes from the second in-plane domain of Cu_2O on Au/Si(111) as previously reported.[35] Figure 10D shows the (222) pole figure of Cu-BTC on Cu_2O/Au/glass with an intense center spot as well as a diffuse ring at $\chi = 70.53°$, which confirmed the out-of-plane order but no in-plane order. The surface morphology of epitaxial and textured Cu-BTC films was determined by plan-view SEM. The Cu-BTC on Cu_2O/Au/Si exhibited in-plane order with well-aligned triangular crystals corresponding to the three-fold symmetry of the (111) plane with two in-plane domains (Figure 10E). The Cu-BTC on Cu_2O/Au/glass showed triangular crystals which were not aligned in-plane, demonstrating out-of-plane order only (Figure 10F).

CONCLUSIONS

In this work, we have demonstrated that epitaxial Cu-BTC(111) films can be electrochemically manufactured from epitaxial Cu_2O(111) with a single in-plane domain that is antiparallel with respect to the Cu_2O precursor. The electrodeposited ordered Cu_2O films could prove to be a low-cost and easily prepared precursor for the fabrication of ordered MOF films on a large scale. Cu-BTC films with a thickness about 740 nm can be produced on Cu_2O/Au or on Au by a complete conversion without the detachment problem

https://doi.org/10.1021/acsami.2c22983
ACS Appl. Mater. Interfaces 2023, 15, 18440−18449

that usually occurs in the electrochemical oxidation of Cu metal to Cu-BTC.[31] We also demonstrated a pathway for epitaxial lift-off of Cu-BTC foils that may provide a path to produce membranes for gas separation and selective sensing. The facile electrochemical strategy exhibits feasibility of epitaxial electro-conversion from oxides to MOFs by oxidation/reduction and should be a general way to fabricate ordered MOF films. For example, by using different linker molecules, it should be possible to attain a wide variety of epitaxial Cu-based MOFs from Cu_2O by electrochemical oxidation. It is also intriguing to use other epitaxial metallic oxides such as Fe_3O_4 and Co_3O_4 to manufacture the corresponding MOFs by electrochemical reduction. As this epitaxial Cu-BTC achieves perfectly oriented pore openings in the [111] direction with in-plane ordering, it is expected to present desirable performance for the selective separation of small-sized gas molecules such as H_2, He, and CO_2. Another interest is that as Cu-BTC can be endowed with conductivity by encapsulating and conjugating with organic guests, the epitaxial Cu-BTC is promising for realizing optimization of electrical properties in electronic devices.

■ ASSOCIATED CONTENT

Supporting Information

The Supporting Information is available free of charge at https://pubs.acs.org/doi/10.1021/acsami.2c22983.

Unit cells and lattice parameters of Cu_2O and Cu-BTC; XRD pattern of Cu-BTC converted from Cu_2O with different thicknesses; XRD pattern, pole figure, and plan-view SEM image of Cu-BTC by complete conversion of 40 nm thick Cu_2O; cross-sectional SEM image of Cu-BTC converted from 40 nm thick Cu_2O and 250 nm thick Cu_2O; XRD pattern, pole figure, and plan-view SEM image of polycrystalline Cu-BTC produced from single-crystal Cu; ATR-FTIR spectra of Cu_2O, oxidized Cu_2O, CuO, and $Cu(OH)_2$; and XRD pattern of CuO powder and Cu-BTC produced from CuO powder (PDF)

■ AUTHOR INFORMATION

Corresponding Author

Jay A. Switzer − *Department of Chemistry and Graduate Center for Materials Research, Missouri University of Science and Technology, Rolla, Missouri 65409-1170, United States;* orcid.org/0000-0002-7332-4634; Email: jswitzer@mst.edu

Authors

Xiaoting Zhang − *Department of Chemistry and Graduate Center for Materials Research, Missouri University of Science and Technology, Rolla, Missouri 65409-1170, United States*

Bin Luo − *Department of Chemistry and Graduate Center for Materials Research, Missouri University of Science and Technology, Rolla, Missouri 65409-1170, United States;* orcid.org/0000-0002-8996-1734

Avishek Banik − *Department of Chemistry and Graduate Center for Materials Research, Missouri University of Science and Technology, Rolla, Missouri 65409-1170, United States;* orcid.org/0000-0001-7269-1929

John Z. Tubbesing − *Department of Chemistry and Graduate Center for Materials Research, Missouri University of Science and Technology, Rolla, Missouri 65409-1170, United States*

Complete contact information is available at: https://pubs.acs.org/10.1021/acsami.2c22983

Notes

The authors declare no competing financial interest.

■ ACKNOWLEDGMENTS

This material was based on work supported by the U.S. Department of Energy, Office of Basic Energy Sciences, Division of Materials Sciences and Engineering, under grant no. DE-FG02-08ER46518.

■ REFERENCES

(1) Bauer, E. G.; Dodson, B. W.; Ehrlich, D. J.; Feldman, L. C.; Flynn, C. P.; Geis, M. W.; Harbison, J. P.; Matyi, R. J.; Peercy, P. S.; Petroff, P. M.; et al. Fundamental Issues in Heteroepitaxy-A Department of Energy, Council on Materials Science Panel Report. *J. Mater. Res.* **1990**, *5*, 852−894.

(2) Stringfellow, G. B. Epitaxy. *Rep. Prog. Phys.* **1982**, *45*, 469−525.

(3) Yaghi, O. M.; Li, G.; Li, H. Selective Binding and Removal of Guests in a Microporous Metal-Organic Framework. *Nature* **1995**, *378*, 703−706.

(4) Yaghi, O. M.; O'Keeffe, M.; Ockwig, N. W.; Chae, H. K.; Eddaoudi, M.; Kim, J. Reticular Synthesis and the Design of New Materials. *Nature* **2003**, *423*, 705−714.

(5) Furukawa, H.; Cordova, K. E.; O'Keeffe, M.; Yaghi, O. M. The Chemistry and Applications of Metal-Organic Frameworks. *Science* **2013**, *341*, 1230444.

(6) Zhang, X.; Lin, R. B.; Wang, J.; Wang, B.; Liang, B.; Yildirim, T.; Zhang, J.; Zhou, W.; Chen, B. Optimization of the Pore Structures of MOFs for Record High Hydrogen Volumetric Working Capacity. *Adv. Mater.* **2020**, *32*, 1907995.

(7) Li, J.-R.; Kuppler, R. J.; Zhou, H.-C. Selective Gas Adsorption and Separation in Metal-Organic Frameworks. *Chem. Soc. Rev.* **2009**, *38*, 1477−1504.

(8) Lee, J.; Farha, O. K.; Roberts, J.; Scheidt, K. A.; Nguyen, S. T.; Hupp, J. T. Metal-Organic Framework Materials as Catalysts. *Chem. Soc. Rev.* **2009**, *38*, 1450−1459.

(9) Wang, C.; An, B.; Lin, W. Metal-Organic Frameworks in Solid-Gas Phase Catalysis. *ACS Catal.* **2018**, *9*, 130−146.

(10) Kreno, L. E.; Leong, K.; Farha, O. K.; Allendorf, M.; Van Duyne, R. P.; Hupp, J. T. Metal-Organic Framework Materials as Chemical Sensors. *Chem. Rev.* **2012**, *112*, 1105−1125.

(11) Yao, M.-S.; Zheng, J. J.; Wu, A. Q.; Xu, G.; Nagarkar, S. S.; Zhang, G.; Tsujimoto, M.; Sakaki, S.; Horike, S.; Otake, K.; et al. A Dual-Ligand Porous Coordination Polymer Chemiresistor with Modulated Conductivity and Porosity. *Angew. Chem., Int. Ed.* **2020**, *59*, 172−176.

(12) Deng, W.-H.; Yao, M.-S.; Zhang, M.-Y.; Tsujimoto, M.; Otake, K.; Wang, B.; Li, C.-S.; Xu, G.; Kitagawa, S. Non-Contact Real-Time Detection of Trace Nitro-Explosives by MOF Composites Visible-Light Chemiresistor. *Natl. Sci. Rev.* **2022**, *9*, nwac143.

(13) Zhang, X.; Chen, A.; Zhong, M.; Zhang, Z.; Zhang, X.; Zhou, Z.; Bu, X.-H. Metal-Organic Frameworks (MOFs) and MOF-Derived Materials for Energy Storage and Conversion. *Electrochem. Energy Rev.* **2019**, *2*, 29−104.

(14) Tu, M.; Fischer, R. A. Heteroepitaxial Growth of Surface Mounted Metal-Organic Framework Thin Films with Hybrid Adsorption Functionality. *J. Mater. Chem. A* **2014**, *2*, 2018−2022.

(15) Liu, B.; Tu, M.; Fischer, R. A. Metal-Organic Framework Thin Films: Crystallite Orientation Dependent Adsorption. *Angew. Chem., Int. Ed.* **2013**, *52*, 3402−3405.

(16) Bux, H.; Feldhoff, A.; Cravillon, J.; Wiebcke, M.; Li, Y.-S.; Caro, J. Oriented Zeolitic Imidazolate Framework-8 Membrane with Sharp H_2/C_3H_8 Molecular Sieve Separation. *Chem. Mater.* **2011**, *23*, 2262−2269.

(17) Liu, B.; Shekhah, O.; Arslan, H. K.; Liu, J.; Wöll, C.; Fischer, R. A. Enantiopure Metal-Organic Framework Thin Films: Oriented

SURMOF Growth and Enantioselective Adsorption. *Angew. Chem., Int. Ed.* **2012**, *51*, 807−810.
(18) Gu, Z.-G.; Grosjean, S.; Bräse, S.; Wöll, C.; Heinke, L. Enantioselective Adsorption in Homochiral Metal-Organic Frameworks: The Pore Size Influence. *Chem. Commun.* **2015**, *51*, 8998−9001.
(19) Xia, W.; Zou, R.; An, L.; Xia, D.; Guo, S. A Metal-Organic Framework Route to in Situ Encapsulation of Co@Co_3O_4@C Core@Bishell Nanoparticles into a Highly Ordered Porous Carbon Matrix for Oxygen Reduction. *Energy Environ. Sci.* **2015**, *8*, 568−576.
(20) Aguilera-Sigalat, J.; Bradshaw, D. Synthesis and Applications of Metal-Organic Framework-Quantum Dot (QD@ MOF) Composites. *Coord. Chem. Rev.* **2016**, *307*, 267−291.
(21) Chen, Z.; Gu, Z.-G.; Fu, W.-Q.; Wang, F.; Zhang, J. A Confined Fabrication of Perovskite Quantum Dots in Oriented MOF Thin Film. *ACS Appl. Mater. Interfaces* **2016**, *8*, 28737−28742.
(22) Yu, J.; Cui, Y.; Xu, H.; Yang, Y.; Wang, Z.; Chen, B.; Qian, G. Confinement of Pyridinium Hemicyanine Dye within an Anionic Metal-Organic Framework for Two-Photon-Pumped Lasing. *Nat. Commun.* **2013**, *4*, 2719.
(23) Falcaro, P.; Okada, K.; Hara, T.; Ikigaki, K.; Tokudome, Y.; Thornton, A. W.; Hill, A. J.; Williams, T.; Doonan, C.; Takahashi, M. Centimetre-Scale Micropore Alignment in Oriented Polycrystalline Metal-Organic Framework Films via Heteroepitaxial Growth. *Nat. Mater.* **2017**, *16*, 342−348.
(24) Chui, S. S.-Y.; Lo, S. M.-F.; Charmant, J. P. H.; Orpen, A. G.; Williams, I. D. A Chemically Functionalizable Nanoporous Material $[Cu_3(TMA)_2(H_2O)_3]_n$. *Science* **1999**, *283*, 1148−1150.
(25) Allendorf, M. D.; Houk, R. J. T.; Andruszkiewicz, L.; Talin, A. A.; Pikarsky, J.; Choudhury, A.; Gall, K. A.; Hesketh, P. J. Stress-Induced Chemical Detection Using Flexible Metal-Organic Frameworks. *J. Am. Chem. Soc.* **2008**, *130*, 14404−14405.
(26) Kung, C.-W.; Audu, C. O.; Peters, A. W.; Noh, H.; Farha, O. K.; Hupp, J. T. Copper Nanoparticles Installed in Metal-Organic Framework Thin Films are Electrocatalytically Competent for CO_2 Reduction. *ACS Energy Lett.* **2017**, *2*, 2394−2401.
(27) Talin, A. A.; Centrone, A.; Ford, A. C.; Foster, M. E.; Stavila, V.; Haney, P.; Kinney, R. A.; Szalai, V.; El Gabaly, F.; Yoon, H. P.; et al. Tunable Electrical Conductivity in Metal-Organic Framework Thin-Film Devices. *Science* **2014**, *343*, 66−69.
(28) Kelso, M. V.; Tubbesing, J. Z.; Chen, Q.; Switzer, J. A. Epitaxial Electrodeposition of Chiral Metal Surfaces on Silicon (643). *J. Am. Chem. Soc.* **2018**, *140*, 15812−15819.
(29) Luo, B.; Banik, A.; Bohannan, E. W.; Switzer, J. A. Epitaxial Electrodeposition of Hole Transport CuSCN Nanorods on Au (111) at the Wafer Scale and Lift-Off to Produce Flexible and Transparent Foils. *Chem. Mater.* **2022**, *34*, 970−978.
(30) Banik, A.; Tubbesing, J. Z.; Luo, B.; Zhang, X.; Switzer, J. A. Epitaxial Electrodeposition of Optically Transparent Hole-Conducting CuI on n-Si (111). *Chem. Mater.* **2021**, *33*, 3220−3227.
(31) Luo, B.; Banik, A.; Bohannan, E. W.; Switzer, J. A. Epitaxial Electrodeposition of Cu (111) onto an L-Cysteine Self-Assembled Monolayer on Au (111) and Epitaxial Lift-Off of Single-Crystal-Like Cu Foils for Flexible Electronics. *J. Phys. Chem. C* **2020**, *124*, 21426−21434.
(32) He, Z.; Gudavarthy, R. V.; Koza, J. A.; Switzer, J. A. Room-Temperature Electrochemical Reduction of Epitaxial Magnetite Films to Epitaxial Iron Films. *J. Am. Chem. Soc.* **2011**, *133*, 12358−12361.
(33) Campagnol, N.; Van Assche, T. R. C.; Li, M.; Stappers, L.; Dincă, M.; Denayer, J. F. M.; Binnemans, K.; De Vos, D. E.; Fransaer, J. On the Electrochemical Deposition of Metal-Organic Frameworks. *J. Mater. Chem. A* **2016**, *4*, 3914−3925.
(34) Shekhah, O.; Wang, H.; Kowarik, S.; Schreiber, F.; Paulus, M.; Tolan, M.; Sternemann, C.; Evers, F.; Zacher, D.; Fischer, R. A.; et al. Step-by-Step Route for the Synthesis of Metal-Organic Frameworks. *J. Am. Chem. Soc.* **2007**, *129*, 15118−15119.
(35) Zheng, R.; Fu, Z. H.; Deng, W. H.; Wen, Y.; Wu, A. Q.; Ye, X. L.; Xu, G. The Growth Mechanism of a Conductive MOF Thin Film in Spray-Based Layer-by-Layer Liquid Phase Epitaxy. *Angew. Chem., Int. Ed.* **2022**, *61*, No. e202212797.
(36) Okada, K.; Mori, K.; Fukatsu, A.; Takahashi, M. Oriented Growth of Semiconducting TCNQ@$Cu_3(BTC)_2$ MOF on $Cu(OH)_2$: Crystallographic Orientation and Pattern Formation toward Semiconducting Thin-Film Devices. *J. Mater. Chem. A* **2021**, *9*, 19613−19618.
(37) Vishnyakov, A.; Ravikovitch, P. I.; Neimark, A. V.; Bülow, M.; Wang, Q. M. Nanopore Structure and Sorption Properties of Cu-BTC Metal-Organic Framework. *Nano Lett.* **2003**, *3*, 713−718.
(38) Switzer, J. A.; Hill, J. C.; Mahenderkar, N. K.; Liu, Y.-C. Nanometer-Thick Gold on Silicon as a Proxy for Single-Crystal Gold for the Electrodeposition of Epitaxial Cuprous Oxide Thin Films. *ACS Appl. Mater. Interfaces* **2016**, *8*, 15828−15837.
(39) Switzer, J. A.; Kothari, H. M.; Poizot, P.; Nakanishi, S.; Bohannan, E. W. Enantiospecific Electrodeposition of a Chiral Catalyst. *Nature* **2003**, *425*, 490−493.
(40) Wu, X.; Bai, H.; Zhang, J.; Chen, F. e.; Shi, G. Copper Hydroxide Nanoneedle and Nanotube Arrays Fabricated by Anodization of Copper. *J. Phys. Chem. B* **2005**, *109*, 22836−22842.
(41) Pan, L.; Liu, Y.; Yao, L.; Ren, D.; Sivula, K.; Grätzel, M.; Hagfeldt, A. Cu_2O Photocathodes with Band-Tail States Assisted Hole Transport for Standalone Solar Water Splitting. *Nat. Commun.* **2020**, *11*, 318.
(42) Omelchenko, S. T.; Tolstova, Y.; Atwater, H. A.; Lewis, N. S. Excitonic Effects in Emerging Photovoltaic Materials: A Case Study in Cu_2O. *ACS Energy Lett.* **2017**, *2*, 431−437.
(43) Chastain, J.; King, R. C., Jr. *Handbook of X-ray Photoelectron Spectroscopy*; Perkin-Elmer Corporation, 1992; Vol. *40*, p 221.